AJNR

NMR of the normal and pathologic eye and orbit.

D F Sobel, C Mills, D Char, D Norman, M Brant-Zawadzki, L Kaufman and L Crooks

AJNR Am J Neuroradiol 1984, 5 (4) 345-350
http://www.ajnr.org/content/5/4/345

NMR of the Normal and Pathologic Eye and Orbit

David F. Sobel[1, 2]
Catherine Mills[1, 3]
Devron Char[4]
David Norman[1]
Michael Brant-Zawadzki[1]
Leon Kaufman[5]
Larry Crooks[5]

Nuclear magnetic resonance (NMR) images of the eye and orbit were reviewed in a series of 100 normals and in four patients with orbital or ocular pathology. A rich retrobulbar fat content rendered the orbit well suited for NMR imaging. The lens, vitreous, optic nerve, and extraocular muscles were well visualized with spin-echo technique. However, NMR spatial resolution was inferior to that of high-resolution computed tomography (CT). NMR was comparable to CT in demonstrating choroidal melanoma and orbital pseudotumor. NMR exhibited a particular sensitivity in displaying tissue contrast for infiltrative orbital fat lesions with a relatively long T1. This initial experience suggests a promising role for NMR in orbital imaging.

The clinical utility of nuclear magnetic resonance (NMR) imaging has been exhibited by many recent reports [1–6]. In the brain, NMR has demonstrated tissue contrast markedly superior to and spatial resolution comparable to that of computed tomography (CT) [7–10]. The purpose of this communication is to present a preliminary evaluation of NMR imaging in the study of the orbit.

Subjects and Methods

One hundred patients with normal orbital and ocular anatomy and four patients with orbital or ocular pathology were studied. The normal images were obtained by studying normal volunteers and patients with suspected intracranial pathology, some of whom have been described by Moseley et al. [11].

NMR images were obtained with a 3.5 kG (0.35 T) superconducting magnet operating at a resonant frequency of 15 MHz. The magnetic field gradients did not exceed 1 G/cm and had a rise time of 1 msec. A head coil with a 25 cm aperture was used. Details of the imaging procedure have been reported [12]. The spin-echo (SE) technique was used with pulse intervals (TRs) of 0.5, 1.0, 1.5, and 2.0 sec. Two echo delay (TE) images at 28 and 56 msec were acquired for each pulse interval sequence. Slice thickness was 7 mm with a slice spacing of about 11 mm. A 0.5 sec TR sequence required 4.3 min and yielded five planes of section. First and second echoes were obtained at each plane of section. A 2.0 sec TR yielded 11 planes of section but required about 17 min. A 2.0 sec TR high-resolution sequence required 34 min. Patients were instructed to restrict head motion but were not asked to restrict eye movement during the imaging sequence. Spatial resolution was 1.7 mm^2 in the xy plane for standard images and 0.8 mm^2 for high resolution. Spatial resolution in the z plane was equal to the slice thickness of 7 mm.

Four patients with orbital or ocular pathology also had CT with a G.E. 8800 scanner. Whereas CT density is dependent on electron density and x-ray attenuation, NMR image intensity is dependent on the factors expressed by the equation, $I = Hf(v) \exp(-TE/T2)(1 - \exp[-TR/T1])$, where I = image intensity, H = local hydrogen density, f(v) is a factor of the fraction and velocity of hydrogen nuclei in motion, TE is the echo delay, T2 is the spin-spin tissue relaxation parameter, TR is the pulse interval, and T1 represents the spin-lattice or longitudinal tissue relaxation parameter [13]. T1 and T2 are exponential tissue characterization parameters dependent on the given tissue and its magnetic molecular environment, whereas TR and TE are computer controlled. Varying TR will affect the relative T1 contribution to

Received September 22, 1983; accepted after revision December 15, 1983.

The opinions and assertions contained herein are the private views of the authors and are not to be construed as official or as reflecting the views of the Department of the Army or the Department of Defense.

Presented at the annual meeting of the American Society of Neuroradiology, San Francisco, June 1983.

This work was supported in part by U.S. Public Health Service grant CA 328S0 from the National Cancer Institute and by Diasonics, Inc.

[1] Department of Radiology, M-396, University of California, San Francisco, CA 94143. Address reprint requests to D. F. Sobel.

[2] Department of Radiology, Letterman Army Medical Center, San Francisco, CA 94129.

[3] Department of Radiology, San Francisco General Hospital, San Francisco, CA 94110.

[4] Department of Ophthalmology, University of California, San Francisco, CA 94143.

[5] Radiology Imaging Laboratory, University of California, San Francisco, CA 94143.

AJNR 5:345–350, July/August 1984
0195–6108/84/0504–0345 $2.00

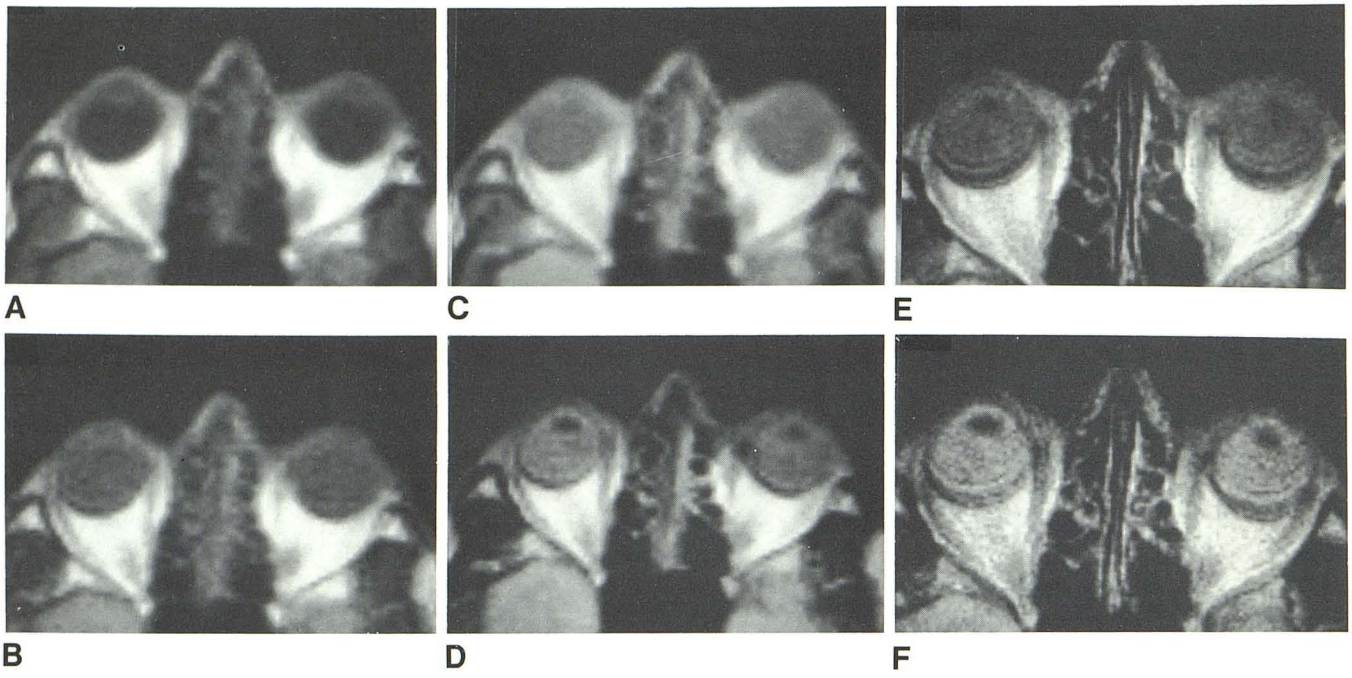

Fig. 1.—Normal subject. NMR SE images. **A,** 0.5 sec TR, 28 msec TE. **B,** 0.5 sec TR, 56 msec TE. **C,** 1.5 sec TR, 28 msec TE. **D,** 1.5 sec TR, 56 msec TE. **E,** 2.0 sec TR, 28 msec TE. **F,** 2.0 sec TR, 56 msec TE. Note high intensity of retrobulbar fat on all imaging sequences. Intensity of lens varies from relatively high at 0.5 sec TR, 28 msec TE to relatively low at 2.0 sec TR, 56 msec TE. Intensity of vitreous displays an inverse tendency to intensity of lens.

tissue contrast, while TE affects the relative T2 contribution. In addition to the SE images, quantitative T1 and T2 images were also obtained. T2 pixel values are calculated from the first and second echo intensities of a given pulse sequence interval. To compute a T1 image, repetition with at least two different TR sequences is necessary. An estimated (T1E) T1 image can be generated from two images with the same TR and different TEs while assuming constant blood flow and hydrogen density [3].

Results

Normal Studies

The rich intraorbital fat content renders the orbit well suited to CT scanning and is also advantageous for NMR imaging. It can be seen from the SE intensity equation that either relatively short T1 or long T2 tissue relaxation times will tend to increase image signal intensity. Since absolute T1 and T2 values vary with the image sequence, magnetic field strength, radiofrequency, and temperature, only relative values will be discussed. Fat, having a very short T1 and intermediate T2, yielded the strongest signal intensity for all values of TR and TE (fig. 1). This was the same as fat imaged elsewhere in the body. The high intensity of fat was useful in differentiating normal from infiltrated tissue but was occasionally detrimental in viewing smaller structures due to spatial blurring.

The osseous orbital wall and adjacent air-containing paranasal sinuses produced the weakest signal intensity due to their relatively low proton density. Extraocular muscles and optic nerve displayed intermediate signal intensity with little variation when TR and TE parameters were varied. The spatial resolution of these structures was generally poor compared with high-resolution CT due to the current lack of thin sections with NMR and the spatial blurring from surrounding fat.

The vitreous represents the major intraglobal component. It is composed of 99% water with small quantities of collagen and hyaluronic acid, giving it a gellike quality [14]. A marked change in vitreous signal intensity was observed when the imaging parameters were varied. Little relative signal was obtained at 0.5 sec TR and 28 msec TE compared with adjacent structures, but a strong relative signal was obtained at the longer TRs and TEs, 2.0 sec TR and 56 msec TE (figs. 1A and 1F). This reflects the relatively long T1 and T2 of the water component. The absolute signal intensity tends to increase with longer TR and decrease with longer TE. However, the images are displayed as relative intensity on the gray scale and not as absolute intensity.

The lens, being 65% water and 35% protein, had a moderate T1 along with a short T2. At short TRs and TEs, 0.5 sec TR and 28 msec TE, the lens yielded a strong signal compared with that of the vitreous, while this relation reversed with a longer TR of 2.0 sec and TE of 56 msec (figs. 1A and 1F).

The sclera and cornea were difficult to identify consistently. This was believed to be due in part to motion of the globe. On 2.0 sec TR high-resolution sequences requiring about 34 min, a rim of low density surrounded the globe, representing motion artifact (figs. 1E and 1F).

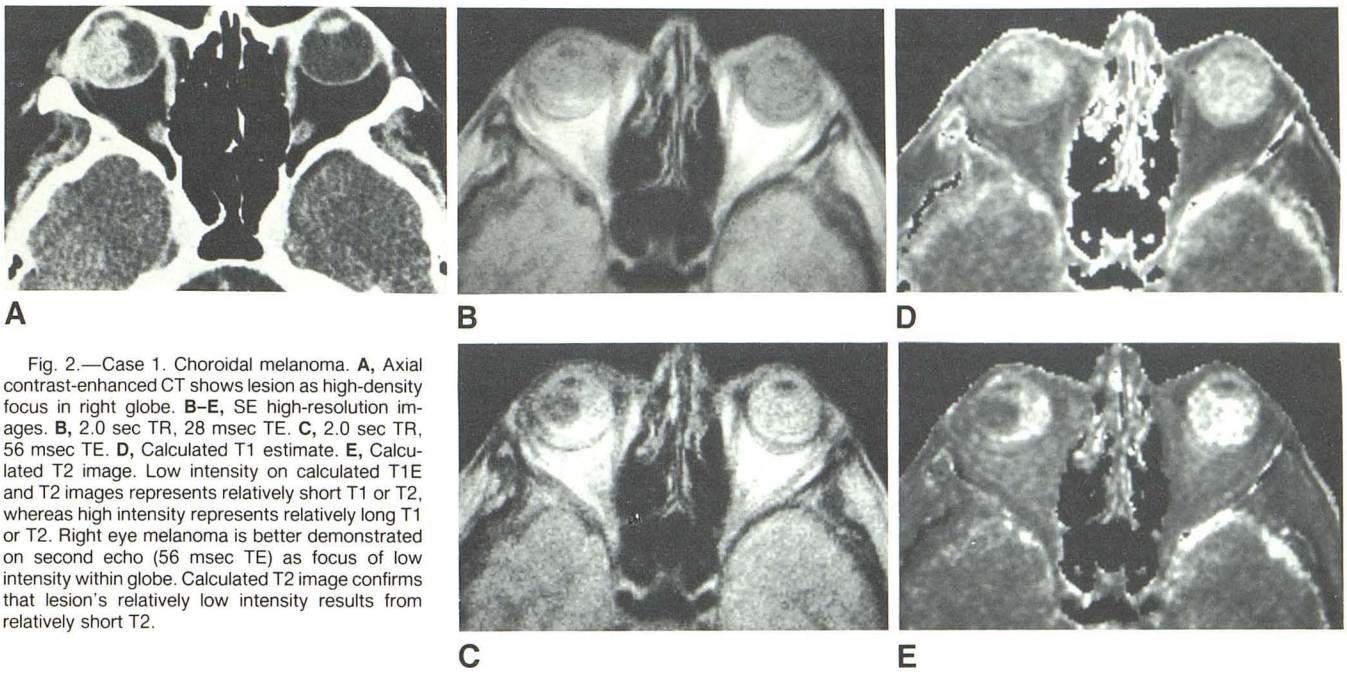

Fig. 2.—Case 1. Choroidal melanoma. **A,** Axial contrast-enhanced CT shows lesion as high-density focus in right globe. **B–E,** SE high-resolution images. **B,** 2.0 sec TR, 28 msec TE. **C,** 2.0 sec TR, 56 msec TE. **D,** Calculated T1 estimate. **E,** Calculated T2 image. Low intensity on calculated T1E and T2 images represents relatively short T1 or T2, whereas high intensity represents relatively long T1 or T2. Right eye melanoma is better demonstrated on second echo (56 msec TE) as focus of low intensity within globe. Calculated T2 image confirms that lesion's relatively low intensity results from relatively short T2.

Pathologic Case Reports

Case 1

A 53-year-old woman had a choroidal melanoma of the right eye (fig. 2). High-resolution 2.0 sec TR images demonstrated the lesion as a focus of relative low intensity. This was better appreciated on the second echo (TE = 56 msec), relating the low signal to a short T2. Calculated T1 and T2 images confirmed the lesion having a short T2 and a short T1. Although a short T1 tended to increase signal intensity, this was overshadowed by the greater T2 effect. The patient was treated with radiotherapy followed by enucleation. NMR demonstrated the lesion as well as CT, where it appeared as a high-density focus.

Case 2

A 13-year-old girl had painless left proptosis. Biopsy demonstrated a sclerosing orbital pseudotumor. NMR revealed infiltration of the lateral rectus, intraorbital fat, and optic nerve (fig. 3). This was seen as an area of low intensity that contrasted to the normal high intensity of fat. This contrast was better shown with a short TR of 0.5 sec, whereas the signal-to-noise ratio and effective spatial resolution were improved at 2.0 sec TR. The low signal intensity was due to a lengthened T1. The absence of change in relative signal intensity between the first and second echoes excluded a T2 effect. NMR was equal to CT in demonstrating the pathology.

Case 3

An 83-year-old man had a painless right-sided proptosis that had developed 6 years after multiple lymph node biopsies had shown benign lymphadenitis. CT showed thickening of the medial rectus, optic nerve, and intraorbital fat (fig. 4A). NMR demonstrated these findings as decreased signal intensity due to the inflammatory mass involving the fat, muscle, and optic nerve (figs. 4B–4G). The abnormal findings were again better contrasted by the 0.5 sec TR than by the 2.0 sec TR sequence, with no change between 28 and 56 msec echoes. Biopsy revealed benign lymphocytic infiltration consistent with orbital pseudotumor.

Case 4

A 12-year-old girl had right proptosis secondary to histologically demonstrable sclerosing orbital pseudotumor. She had also been treated for hyperthyroidism. NMR images with 0.5 sec TR and 1.5 sec TR showed diffuse infiltration of the retrobulbar fat as a relative decrease in intensity compared with the normal left eye. Calculated T1E and T2 images related the findings to a lengthened T1 with little demonstrable change in T2. On CT the infiltrated fat appeared as increased density compared with low attenuation values of normal fat. The findings were equally evident with both techniques.

Discussion

The advent of high-resolution CT with thin sections and multiplanar reformations has allowed diagnosis of orbital pathology with a very high degree of accuracy [15]. The evolution of any new modality in imaging of the orbit must include comparison with CT.

The choroidal melanoma represented the only intraocular mass that we evaluated. The lesion was seen equally well on both CT and NMR. A relatively short T1 and T2 for melanoma was described by Damadian et al. [18] as being characteristic of this lesion and is due to the paramagnetic properties of melanin. We observed a relatively short T1 and T2 in this neoplasm, while most neoplasms demonstrate a relatively long T1 and T2 [16–20]. Currently available diagnostic methods are not useful in predicting the response of uveal melanoma to therapy. It is possible that therapeutic effect may

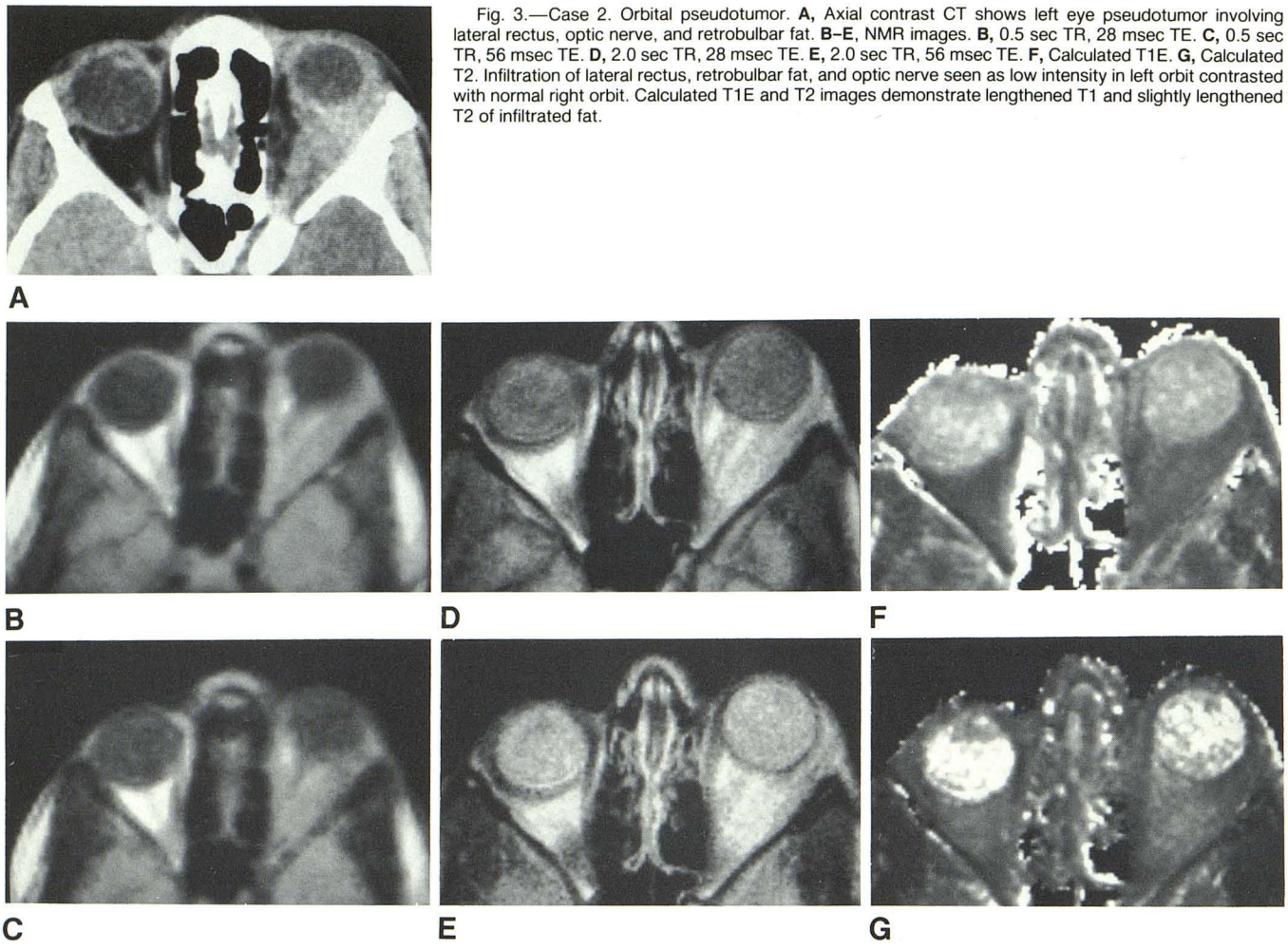

Fig. 3.—Case 2. Orbital pseudotumor. **A,** Axial contrast CT shows left eye pseudotumor involving lateral rectus, optic nerve, and retrobulbar fat. **B–E**, NMR images. **B,** 0.5 sec TR, 28 msec TE. **C,** 0.5 sec TR, 56 msec TE. **D,** 2.0 sec TR, 28 msec TE. **E,** 2.0 sec TR, 56 msec TE. **F,** Calculated T1E. **G,** Calculated T2. Infiltration of lateral rectus, retrobulbar fat, and optic nerve seen as low intensity in left orbit contrasted with normal right orbit. Calculated T1E and T2 images demonstrate lengthened T1 and slightly lengthened T2 of infiltrated fat.

correlate with T1 and T2 tissue characterization parameters and this may have prognostic implications.

We report three patients with pseudotumor of the orbit. One of these patients also had systemic hyperthyroidism. Pseudotumor is an inflammatory reaction that can vary from vasculitis to fibrotic sclerosis to a generalized lymphocytic infiltration. Edema of the involved tissue occurs as part of the inflammatory response. Herfkens et al. [13] reported a direct proportion between H_2O content and the rate constants 1/T1 and 1/T2 for normal and abnormal tissues in the rat, with the exception that the T2 of fat was very long for its water content. The lengthened T1 in orbital pseudotumor is most likely explained by increased water content. The slight demonstrable change in the T2 value of fat involved by pseudotumor tends to support the lack of a direct proportion between fat T2 and H_2O content.

In thyroid ophthalmopathy the pathologic findings are due to a deposition of mucopolysaccharides accounting for an increased water content. There is also infiltration of plasma cells and lymphocytes with an increase in the orbital connective tissue. T1 and T2 tissue parameters will probably not be helpful in differentiating pseudotumor and thyroid ophthalmopathy, but may be useful in distinguishing benign from malignant causes of orbit infiltration. Further study in this regard is required.

In our four pathologic cases, the abnormal findings were equally discernible with both NMR and CT. The ability of NMR to differentiate normal and pathologic orbital tissue was equal but not superior to that of CT. This is in contrast to NMR's superiority in brain imaging. This is because orbital fat exhibits much greater tissue contrast than the brain with CT. It is evident from the normal orbits studied by NMR that spatial resolution, at present, still lags behind high-resolution CT performed with thin sections. Hawkes et al. [21] reported similar limitations of spatial resolution in their evaluation of orbital tumors.

One advantage of NMR imaging of the orbit is the lack of ionizing radiation. This is significant in patients who may

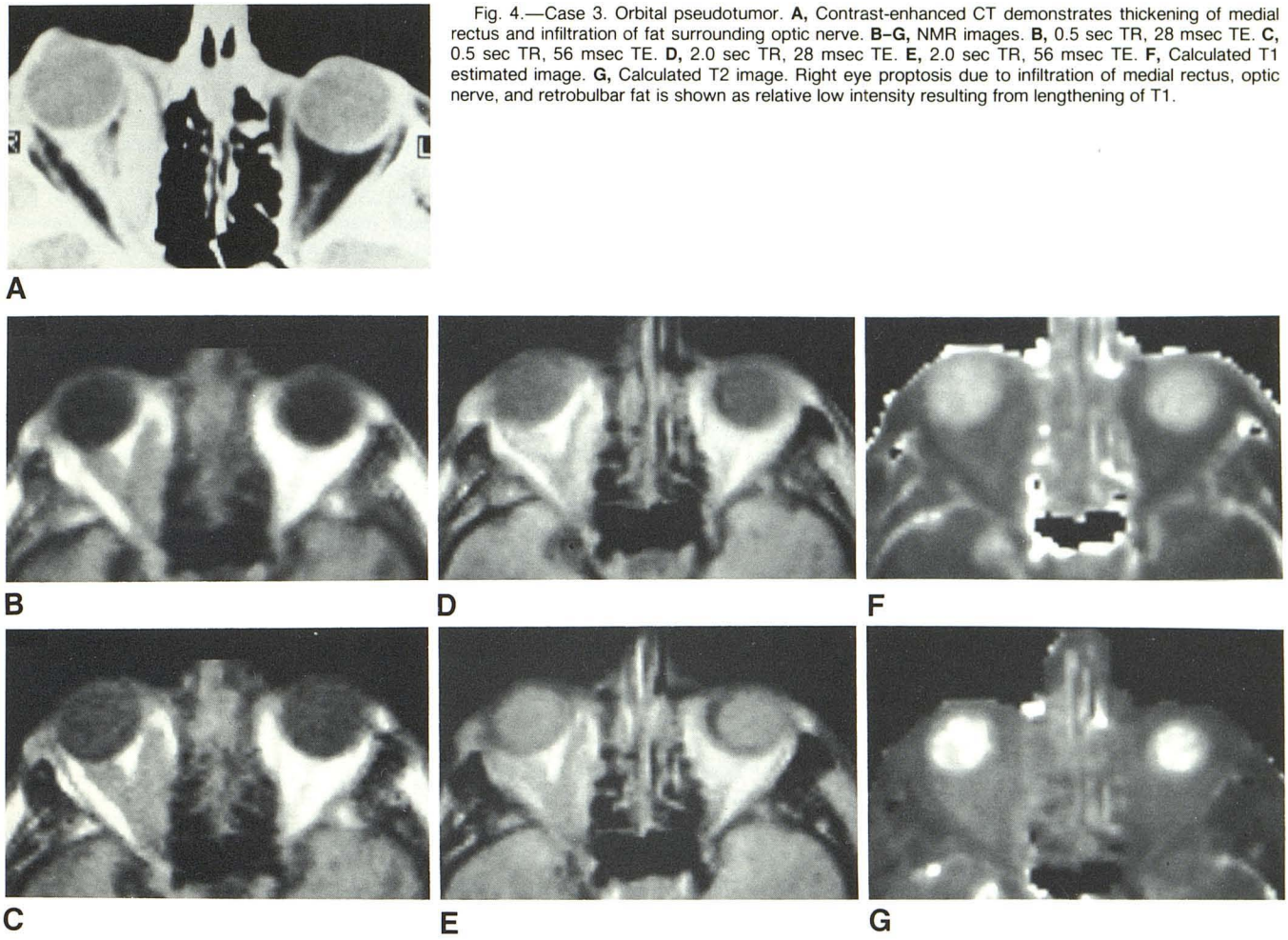

Fig. 4.—Case 3. Orbital pseudotumor. **A,** Contrast-enhanced CT demonstrates thickening of medial rectus and infiltration of fat surrounding optic nerve. **B–G,** NMR images. **B,** 0.5 sec TR, 28 msec TE. **C,** 0.5 sec TR, 56 msec TE. **D,** 2.0 sec TR, 28 msec TE. **E,** 2.0 sec TR, 56 msec TE. **F,** Calculated T1 estimated image. **G,** Calculated T2 image. Right eye proptosis due to infiltration of medial rectus, optic nerve, and retrobulbar fat is shown as relative low intensity resulting from lengthening of T1.

require repeated follow-up studies. Further availability of T1 and T2 tissue parameters affords a new method of examining tissue pathology. In addition, the ability of NMR in determining relative blood flow may prove useful for vascular lesions of the orbit.

A disadvantage of NMR is the current lack of thin sections. Thinner sections will become available in the future with improvements in power supply efficiency and field gradients. The problem of spatial blurring of smaller structures due to the high intensity of fat should be solved with software developments in image intensity scaling. Another problem is that of motion artifact from movement of the globe. This is because data acquisition for each section occurs throughout the imaging sequence. Coronal, sagittal, and oblique reformations have been indispensable in orbital CT. Although NMR allows direct coronal and sagittal imaging, this must be specified before imaging with our system. Retrospective viewing in a plane orthogonal to that originally scanned is not yet available to us. The computer contains three-dimensional voxel information, and future software developments will allow for retrospective viewing in any imaging plane.

REFERENCES

1. James AE Jr, Partain CL, Holland GN, et al. Nuclear magnetic resonance imaging: the current state. *AJR* **1981**;138:201–210
2. Young IR, Bailes DR, Burl M, et al. Initial clinical evaluation of a whole body nuclear magnetic resonance (NMR) tomograph. *J Comput Assist Tomogr* **1982**;6:1–18
3. Crooks LE, Ortendahl DA, Kaufman L, et al. Clinical efficiency of nuclear magnetic resonance imaging. *Radiology* **1983**;146:123–128
4. Young IR, Hall AS, Pallis CA, Bydder GM, Legg NJ, Steiner RE. Nuclear magnetic resonance imaging of the brain in multiple sclerosis. *Lancet* **1981**;2:1063–1066
5. Herfkens RJ, Higgins CB, Hricak H, et al. Nuclear magnetic resonance imaging of the cardiovascular system: normal and pathologic findings. *Radiology* **1983**;147:749–759
6. Hricak H, Williams RD, Moon KL, et al. Nuclear magnetic reso-

nance imaging of the kidney: renal masses. *Radiology* **1983**;147:765–772
7. Young IR, Burl M, Clarke GJ, et al. Magnetic resonance properties of hydrogen: imaging the posterior fossa. *AJNR* **1981**;2:487–493, *AJR* **1981**;137:895–901
8. Bydder GM, Steiner RE, Young IR, et al. Clinical NMR imaging of the brain: 140 cases. *AJNR* **1982**; 3:459–480, *AJR* **1982**; 139:215–236
9. Crooks LE, Mills CM, Davis PL, et al. Visualization of cerebral and vascular abnormalities by NMR imaging. The effects of imaging parameters on contrast. *Radiology* **1982**;144:843–852
10. Brant-Zawadzki M, Davis PL, Crooks L, et al. NMR in the visualization of cerebral abnormalities: comparison with CT. *AJNR* **1983**;4:117–124, *AJR* **1983**;140:847–854
11. Moseley I, Brant-Zawadzki M, Mills C. Nuclear magnetic resonance imaging of the orbit. *Br J Ophthalmol* **1983**;67:333–342
12. Crooks L, Arakawa M, Hoenninger J, et al. Nuclear magnetic resonance whole-body imager operating at 3.5 KGauss. *Radiology* **1982**;143:169–174
13. Herfkens R, Davis P, Crooks L, et al. Nuclear magnetic resonance of the abnormal live rat and correlations with tissue characteristics. *Radiology* **1981**;141:211–218
14. Vaughan D, Asbury T. *General ophthalmology*. Los Altos, CA: Lange, **1977**
15. Char DM, Norman D. The use of computed tomography and ultrasonography in the evaluation of orbital masses. *Surv Ophthalmol* **1982**;17:49–63
16. Damadian R. Tumor detection by nuclear magnetic resonance. *Science* **1971**;171:1151–1153
17. Hollis DP, Economou JS, Parks LC, Eggleston JC, Saryan LA, Czeisler JL. Nuclear magnetic resonance studies of several experimental and human malignant tumors. *Cancer Res* **1973**;33:2156–2160
18. Damadian R, Zaner K, Hor D. Brain tumors by NMR. *Physiol Chem Phys* **1973**;5:381–402
19. Davis PL, Kaufman L, Crooks L, Miller T. Detectability of hepatomas in rat liver by nuclear magnetic resonance imaging. *Invest Radiol* **1981**;16:354–359
20. Davis PL, Sheldon MT, Kaufman L, et al. Nuclear magnetic resonance imaging of mammary adenocarcinomas in the rat. *Cancer* **1983**;51:433–439
21. Hawkes RC, Holland GN, Moore WS, Rizk S, Worthington BS, Kean DM. NMR imaging in the evaluation of orbital tumors. *AJNR* **1983**;4:254–256.